Engineering Analysis with Boundary Elements ▮ (▮▮▮▮) ▮▮▮–▮▮▮

Contents lists available at ScienceDirect

Engineering Analysis with Boundary Elements

journal homepage: www.elsevier.com/locate/enganabound

Three-dimensional stress intensity factors of a central square crack in a transversely isotropic cuboid with arbitrary material orientations

Chao-Shi Chen [a,*], Chia-Hau Chen [a], Ernian Pan [b]

[a] Department of Resources Engineering, National Cheng Kung University, Tainan 701, Taiwan
[b] Department of Civil Engineering, University of Akron, Akron, OH 44325-3905, USA

ARTICLE INFO

Article history:
Received 6 February 2008
Accepted 2 June 2008

Keywords:
Dual-BEM
Single-domain BEM
Transverse isotropy
Three dimensions
Stress intensity factor
Crack opening displacement
Rock anisotropy

ABSTRACT

In this paper, we present the dual boundary element method (dual-BEM) or single-domain BEM to analyze the mixed three-dimensional (3D) stress intensity factors (SIFs) in a finite and transversely isotropic solid containing an internal square crack. The planes of both the transverse isotropy and square crack can be oriented arbitrarily with respect to a fixed global coordinate system. A set of four special nine-node quadrilateral elements are utilized to approximate the crack front as well as the outer boundary, and the mixed 3D SIFs are evaluated using the asymptotic relation between the SIFs and the relative crack opening displacements (COD) via the Barnett–Lothe tensor.

Numerical examples are presented for a cracked cuboid which is transversely isotropic with any given orientation and is under a uniform vertical traction on its top and bottom surfaces. The square crack is located in the center of the cuboid but is oriented arbitrarily. Our results show that among the selected material and crack orientations, the mode-I SIF reaches the largest possible value when the material inclined angle $\psi_1 = 45^\circ$ and dig angle $\beta_1 = 45^\circ$, and the crack inclined angle $\psi_2 = 0^\circ$ and dig angle $\beta_2 = 0^\circ$. It is further observed that when the crack is oriented vertically or nearly vertically, the mode-I SIF becomes negative, indicating that the crack closes due to an overall compressive loading normal to the crack surface. Variation of the SIFs for modes II and III along the crack fronts also shows some interesting features for different combinations of the material and crack orientations.

1. Introduction

Rock fracture mechanics is essentially an extension of the classic fracture mechanics in solids [1,2], which recognizes the importance of the stress intensity near a crack tip. Irwin [2] introduced the stress intensity factors (SIFs) to describe the stress and displacement fields near a crack tip. As is well known, there are three basic crack propagation modes in the fracture process: opening (mode I), sliding (mode II), and tearing (mode III), and furthermore, mechanical safety of a solid elastic structure can be analyzed based on these SIFs. Therefore, determination of SIFs near the crack front in linear elastic fracture mechanics has been always an interesting but challenging task. While most previous studies in SIFs were focused on one or two fracture modes, mixed three-dimensional (3D) modes need to be considered as materials could mostly fail under combined tensile/compressive, shearing, and tearing loads. For 3D isotropic elastic materials, Singh et al. [3] obtained the SIFs using the concept of a universal crack closure integral. For transversely isotropic, orthotropic, and anisotropic solids, Pan and Yuan [4] presented the general relationship between the SIF and the relative crack opening displacement (COD). Lazarus et al. [5] compared the calculated SIFs with experimental results for brittle solids under mixed mode I–III or I–II–III loadings. The 3D SIFs were also calculated by Zhou et al. [6] using the variable-order singular boundary element. More recently, Yue et al. [7] employed the dual boundary element method (dual-BEM) in their calculation of the 3D SIFs of an inclined square crack within a bi-material cuboid. We point out that the dual-BEM was originally proposed by Hong and Chen [8] as reviewed in [9]. Other recent representative works in this direction are those by Ariza and Dominguez [10], Liu et al. [11], Hatzigeorgiou and Beskos [12], Partheymüller et al. [13], Popov et al. [14], Zhao et al. [15], Lo et al. [16], dell'Erba and Aliabadi [17], and Blackburn [18]. The weakly singular and weak-form integral equation method recently proposed by Rundamornrat [19] and Rungamornrat and Mear [20] is also very efficient in crack analysis in anisotropic media. Besides the analytical (integral equation) and BEM methods [21], other common methods, such as the finite difference (FD) [22–24] and the finite element (FE) [25,26], were also applied for 3D SIF analysis. Since both the FD and FE methods require discretization of the whole problem domain,

* Corresponding author.
E-mail addresses: chencs@mail.ncku.edu.tw (C.-S. Chen), pan2@uakron.edu (E. Pan).

0955-7997/$ - see front matter © 2008 Elsevier Ltd. All rights reserved.
doi:10.1016/j.enganabound.2008.06.001

these methods could be time consuming and more expensive than the BEM in fracture analysis.

In this paper, we apply the dual-BEM or the single-domain BEM to analyze the mixed 3D SIFs in a finite and transversely isotropic solid containing an internal square crack. Both the transversely isotropic plane and square crack plane can be oriented arbitrarily with respect to a fixed global coordinate system. A set of special nine-node quadrilateral elements are utilized to approximate the crack surface as well as the outer boundary, and the mixed 3D SIFs are evaluated using the asymptotic relation between the SIFs and the relative CODs via the Barnett–Lothe tensor. Our numerical examples show clearly the strong dependence of 3D SIFs on both the material and crack orientations, and these results could be useful in fracture analysis and design of anisotropic elastic solids.

The paper is organized as follows: in Section 2, we briefly present the required basic equations, including the related local and global coordinate systems. In Section 3, the two important BEM equations are presented for the modeling of a cracked 3D anisotropic cuboid: One is the displacement BEM and another is the traction BEM. The special crack front elements and the corresponding formulation for the mixed SIF calculation are presented in Section 4, and detailed numerical results are discussed in Section 5. Finally, conclusions are drawn in Section 6.

2. Basic equations

We consider a transversely isotropic elastic finite domain with arbitrarily oriented transverse isotropy plane. Inside this domain, there is a central square crack, which is also oriented arbitrarily. First, shown in Fig. 1 is the relation between the global coordinates (x,y,z) or (x_1,x_2,x_3) and the local transversely isotropic material coordinate system x', y', and z', where z' is along the symmetry axis of the material, and $(x'-y')$ is parallel to the isotropic plane. The inclined angle ψ_1 is defined as the angle between the global horizontal plane and the isotropic plane of the material, and the dip orientation β_1 is defined as the angle between the inclined angle plane and the global y-axis.

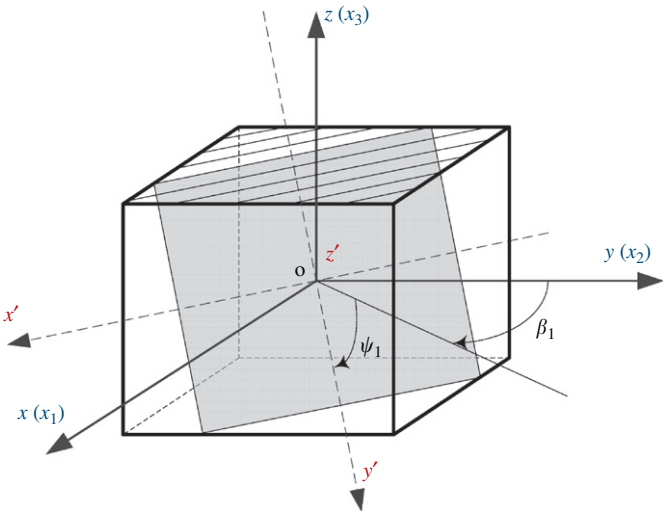

Fig. 1. Relation between the local (x',y',z') and global (x,y,z) coordinate systems where the local z'-axis is along the symmetry axis of the transversely isotropic material. In other words, the local (x',y')-plane is parallel to the isotropic plane of the material; ψ_1 is the inclined angle between the global horizontal plane (x,y) and the local isotropic plane (x',y'); β_1 is the dip orientation between the global y-axis and the include plane.

It is obvious that the transformation between the local (x',y',z') and global (x,y,z) coordinates can be described by the following relation:

$$\begin{bmatrix} x' \\ y' \\ z' \end{bmatrix} = \begin{bmatrix} \cos\beta_1 & -\sin\beta_1 & 0 \\ \cos\psi_1 \sin\beta_1 & \cos\psi_1 \cos\beta_1 & -\sin\psi_1 \\ \sin\psi_1 \sin\beta_1 & \sin\psi_1 \cos\beta_1 & \cos\psi_1 \end{bmatrix} \begin{bmatrix} x \\ y \\ z \end{bmatrix} \tag{1}$$

To solve the problem using the BEM formulation, we first present the governing equations in linear elasticity.

(1) Equations of equilibrium:

$$\sigma_{ij,j} + b_i = 0, \quad i,j = 1,2,3 \tag{2}$$

where σ_{ij} is the stress tensor; b_i the body force component; and subscript "$,j$" denotes partial differentiation with respect to the global coordinates x, y, and z.

(2) Constitutive relation:

$$[\varepsilon] = [a][\sigma] \tag{3}$$

where

$$[\varepsilon] = [\varepsilon_{11}, \varepsilon_{22}, \varepsilon_{33}, 2\varepsilon_{23}, 2\varepsilon_{13}, 2\varepsilon_{12}]^{\mathrm{t}} \tag{4}$$

is the strain in the column matrix form, and

$$[\sigma] = [\sigma_{11}, \sigma_{22}, \sigma_{33}, \sigma_{23}, \sigma_{13}, \sigma_{12}]^{\mathrm{t}} \tag{5}$$

is the stress in the column matrix form. Also in Eq. (3), $[a]$ is the elastic compliance matrix of the anisotropic elastic solid. For the transversely isotropic material, there are five independent elastic parameters (E, E', ν, ν', and G') in the matrix $[a]$. The definitions of these moduli are: E and E' are the Young's moduli in the plane of transverse isotropy and in a direction normal to it, respectively; ν and ν' are the Poisson's ratios characterizing the lateral strain response in the plane of transverse isotropy to a stress acting parallel and normal to it, respectively; G' is the shear modulus normal to the plane of transverse isotropy. Furthermore, the shear modulus G in the plane of transverse isotropy is equal to $E/(2(1+\nu))$. For the transversely isotropic material oriented arbitrarily with respect to the global coordinate system, the matrix $[a]$ will also be a function of the inclined angle ψ_1 and dip orientation β_1. As an example, Appendix A lists the elements of $[a]$ when $\beta_1 = 0$ [27]. It is further observed from Appendix A that the coefficients a_{15}, a_{25}, a_{35}, and a_{46} are zero when ψ_1 is equal to 0° or 90°.

(3) Strain–displacement relation:

$$\varepsilon_{ij} = 0.5(u_{i,j} + u_{j,i}), \quad i,j = 1,2,3 \tag{6}$$

where u_i are the elastic displacements.

3. Single-domain boundary integral equations

We now present the basic relations in the boundary element analysis for fracture problems in linear elasticity. It is based on the dual-BEM [8,9] or the single-domain BEM [28] approach.

We assume that the finite domain under consideration is free of any body force (i.e., $b_i = 0$ in Eq. (2)) and is bounded by an outer boundary S with given boundary conditions. Inside its domain, there is a crack described by its surface Γ (where $\Gamma = \Gamma^+ = -\Gamma^-$, with superscripts "+" and "−" denoting the positive and negative sides of the crack). We further assume that the tractions on both sides of the crack are equal and opposite. Then the single-domain BEM formulation consists of the following displacement and traction boundary integral equations [29].

Please cite this article as: Chen C-S, et al. Three-dimensional stress intensity factors of a central square crack in a transversely isotropic cuboid with arbitrary material orientations. Eng Anal Bound Elem (2008), doi:10.1016/j.enganabound.2008.06.001

(1) Displacement boundary integral equations

$$b_{ij}u_j(\mathbf{y}_S) + \int_S T^*_{ij}(\mathbf{y}_S,\mathbf{x}_S)u_j(\mathbf{x}_S)\,dS(\mathbf{x}_S) - \int_S U^*_{ij}(\mathbf{y}_S,\mathbf{x}_S)T_j(\mathbf{x}_S)\,dS(\mathbf{x}_S) = -\int_\Gamma T^*_{ij}(\mathbf{y}_S,\mathbf{x}_{\Gamma^+})[u_j(\mathbf{x}_{\Gamma^+}) - u_j(\mathbf{x}_{\Gamma^-})]\,d\Gamma(\mathbf{x}_{\Gamma^+}) \quad (7)$$

where b_{ij} are coefficients that depend only on the local geometry of the uncracked boundary at $\mathbf{y}_S$. A point on the positive (or negative) side of the crack is denoted by $\mathbf{x}_{\Gamma^+}$ (or $\mathbf{x}_{\Gamma^-}$), and on the uncracked boundary by both $\mathbf{x}_S$ and $\mathbf{y}_S$. Also in Eq. (7), u_j and T_j represent the displacements and tractions on the boundary (or crack surface), and U^*_{ij} and T^*_{ij} are the Green's functions for displacements and tractions in a general anisotropic elastic solid [4], respectively. A practical material case that will be studied in detail in this paper is the transversely isotropic material with arbitrary material orientation with respect to the global coordinates. We also point out that the first integral on the left-hand side of Eq. (7) has a strong singularity, which will be treated by the rigid-body motion method. At the same time, the calculation of b_{ij} can also be avoided. The second term on the left-hand side has only a weak singularity, and thus, is integrable.

(2) Traction boundary integral equations

$$\frac{[T_l(\mathbf{y}_{\Gamma^+}) - T_l(\mathbf{y}_{\Gamma^-})]}{2} + n_m(\mathbf{y}_{\Gamma^+}) \times \int_S c_{lmik}T^*_{ij,k}(\mathbf{y}_{\Gamma^+},\mathbf{x}_S)u_j(\mathbf{x}_S)\,dS(\mathbf{x}_S) + n_m(\mathbf{y}_{\Gamma^+}) \times \int_\Gamma c_{lmik}T^*_{ij,k}(\mathbf{y}_{\Gamma^+},\mathbf{x}_{\Gamma^+})[u_j(\mathbf{x}_{\Gamma^+}) - u_j(\mathbf{x}_{\Gamma^-})]\,d\Gamma(\mathbf{x}_{\Gamma^+}) = n_m(\mathbf{y}_{\Gamma^+})\int_S c_{lmik}U^*_{ij,k}(\mathbf{y}_{\Gamma^+},\mathbf{x}_S)T_j(\mathbf{x}_S)\,dS(\mathbf{x}_S) \quad (8)$$

where n_m is the unit outward normal of the positive side of the crack surface at $\mathbf{y}_{\Gamma^+}$ and c_{lmik} is the fourth-order stiffness tensor of the anisotropic medium; $U^*_{ij,k}$ and $T^*_{ij,k}$ are the derivatives of the Green's displacements and tractions with respect to the source point, respectively [30].

Eqs. (7) and (8) form a pair of boundary integral equations, called single-domain BEMs, and they can be applied to generally anisotropic media. They can be discretized and solved numerically for unknown boundary displacements (or the relative CODs on the crack surface) and tractions. However, before we apply these single-domain BEMs to calculate the mixed SIFs, we first briefly present the special elements and the approach for the evaluation of 3D SIF.

4. Different types of boundary/crack elements and SIF expressions

In order to discretize both the boundary and crack surface, the nine-node quadrilateral curved elements are used [4]. There are four types of elements, with type I for the uncracked boundary or the interior of the crack surface, and the other three types for different crack fronts (types II–IV), as shown in Fig. 2.

First, the global coordinates x_i at any point within the element are expressed as

$$x_i = \sum_{j=1}^{9}\phi_j x_i^j, \quad i = 1,2,3 \quad (9)$$

where the subscript i denotes the component of nodal coordinates and the superscript j denotes the number of nodes. The shape functions ϕ_j ($j = 1$–9) are functions of the intrinsic coordinates (ξ_1, ξ_2), and their expressions for different elements are listed in Appendix B.

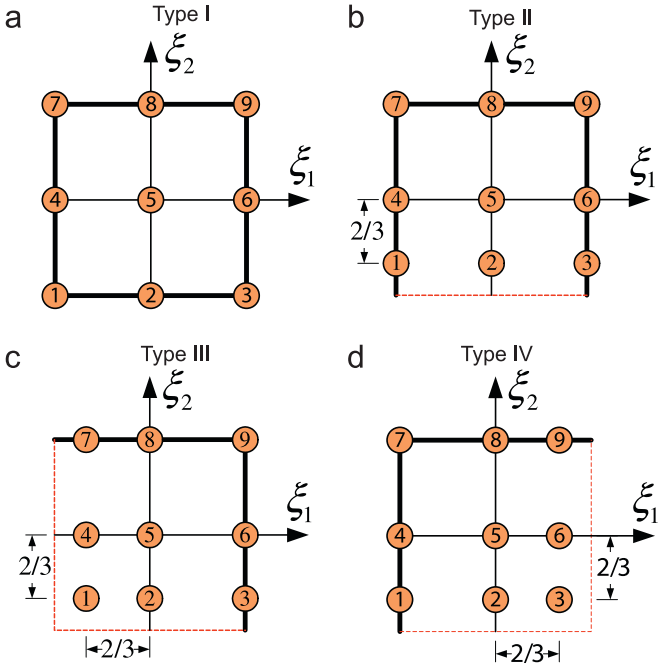

Fig. 2. Four different types of elements for the uncracked boundary and the crack surface.

Similarly, the displacements u_i, and traction T_i on the uncracked boundary, and the relative COD Δu_i ($\Delta u_i = u_i^{\Gamma^+} - u_i^{\Gamma^-}$) on the crack surface can be approximated as

$$u_i = \sum_{j=1}^{9}\phi_j u_i^j, \quad T_i = \sum_{j=1}^{9}\phi_j T_i^j, \quad \Delta u_i = \sum_{j=1}^{9}\phi_j \Delta u_i^j, \quad i = 1,2,3 \quad (10)$$

However, for the relative COD on the crack element near a crack front, weight functions need to be multiplied for accurate evaluation of the SIFs. It is well known that for a crack in a homogeneous and anisotropic solid, the relative COD is proportional to $\sqrt{r}$, where r is the distance behind the crack tip (front). Therefore, for element types II–IV (Fig. 2), we employ the following approximation for the relative COD:

$$\Delta u_i = \sum_{j=1}^{9}\sqrt{(1+\xi_2)}\phi_j \Delta u_i^j, \quad i = 1,2,3 \quad (11)$$

$$\Delta u_i = \sum_{j=1}^{9}\sqrt{(1+\xi_1)(1+\xi_2)}\phi_j \Delta u_i^j, \quad i = 1,2,3 \quad (12)$$

$$\Delta u_i = \sum_{j=1}^{9}\sqrt{(1-\xi_1)(1+\xi_2)}\phi_j \Delta u_i^j, \quad i = 1,2,3 \quad (13)$$

where the corresponding shape functions ϕ_j given in Appendix B should be used correspondingly.

Once the relative CODs are solved in the global coordinates, they can be transformed to the local coordinates (or the crack-tip coordinates) to find the SIFs. Assume that the crack front is smooth and that the crack tip is away from the corner; then the singular term in the asymptotic expansion of the displacement field near the crack tip (front) satisfies the generalized plane strain condition in the local coordinates. Actually, if we let r be the distance behind the crack front, then in terms of the relative CODs in the crack-tip coordinate, the

Please cite this article as: Chen C-S, et al. Three-dimensional stress intensity factors of a central square crack in a transversely isotropic cuboid with arbitrary material orientations. Eng Anal Bound Elem (2008), doi:10.1016/j.enganabound.2008.06.001

three SIFs can be expressed as follows:

$$\begin{Bmatrix} K_{II} \\ K_I \\ K_{III} \end{Bmatrix} = 2\sqrt{\frac{2r}{\pi}}\mathbf{L}^{-1}\begin{Bmatrix} \Delta u_1 \\ \Delta u_2 \\ \Delta u_3 \end{Bmatrix}, \tag{14}$$

where **L** is the Barnett–Lothe tensor [31], which depends only on the anisotropic properties of the solid in the crack front coordinates. The normalized SIFs (F_I, F_{II}, and F_{III}) can be calculated as follows:

$$\begin{Bmatrix} F_I \\ F_{II} \\ F_{III} \end{Bmatrix} = T^{-1}\sqrt{\frac{1}{\pi a}}\begin{Bmatrix} K_I \\ K_{II} \\ K_{III} \end{Bmatrix} \tag{15}$$

where a is the half crack length and T the applied vertical traction in the problem to be discussed below. We also point out that r in Eq. (14) was selected to be $0.00001a$ in our numerical calculation.

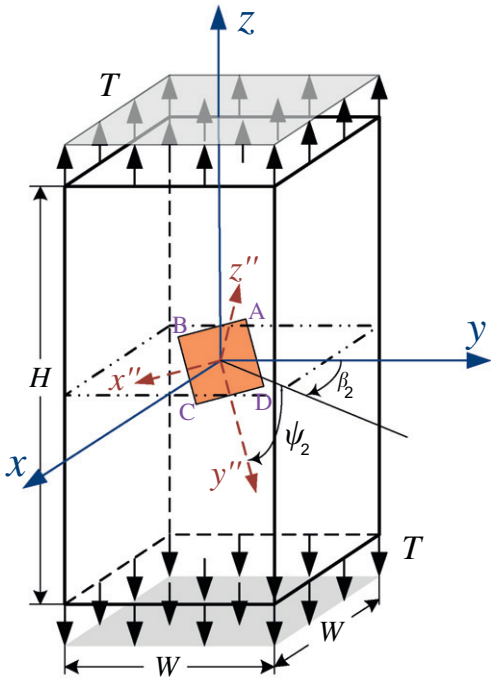

Fig. 3. A central square crack (ABCD: $2a \times 2a$) within a finite cuboid $W \times W \times H$ under a uniform normal stress T in the vertical direction. The orientation of the square crack is described by the inclined angle ψ_2 and dip orientation β_2.

5. Numerical results and discussion

Consider a linearly elastic, homogeneous, and transversely isotropic cuboid with dimension $W \times W \times H$, as shown in Fig. 3. Let x, y, and z (or x_1, x_2, and x_3) be the global Cartesian coordinates

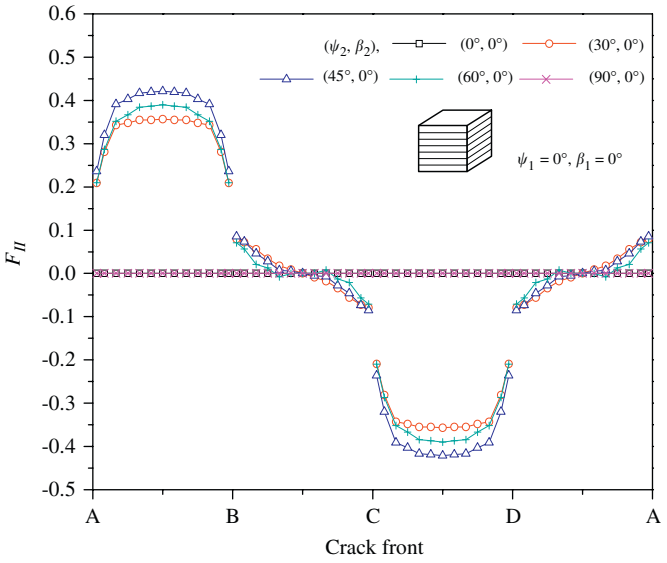

Fig. 5. The normalized mode-II SIF along the square-shaped crack fronts AB, BC, CD, and DA for different crack orientation (ψ_2, β_2) within a finite transversely isotropic cuboid. The material orientation is fixed at $(\psi_1 = 0°, \beta_1 = 0°)$.

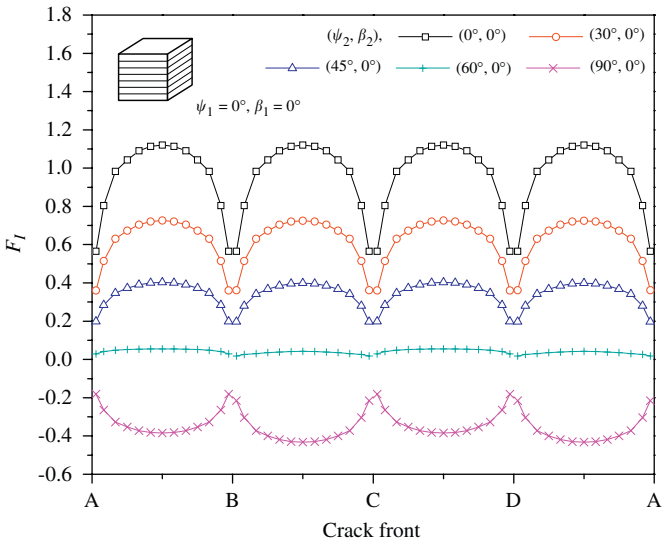

Fig. 4. The normalized mode-I SIF along the square-shaped crack fronts AB, BC, CD, and DA for different crack orientation (ψ_2, β_2) within a finite transversely isotropic cuboid. The material orientation is fixed at $(\psi_1 = 0°, \beta_1 = 0°)$.

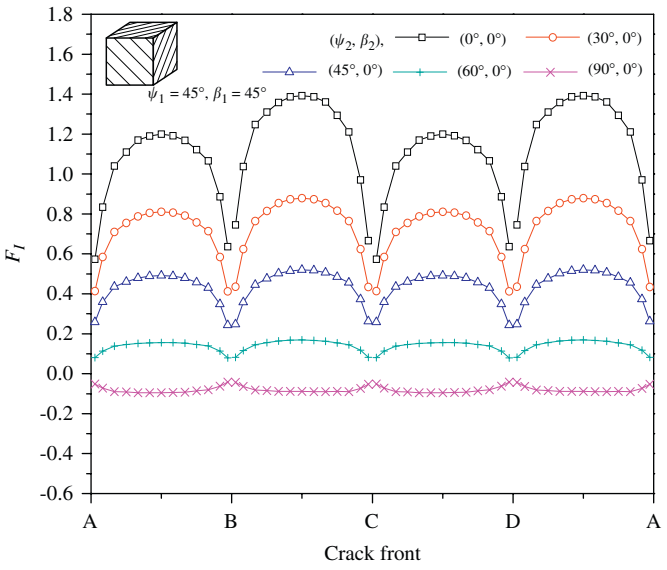

Fig. 6. The normalized mode-I SIF along the square-shaped crack fronts AB, BC, CD, and DA for different crack orientation (ψ_2, β_2) within a finite transversely isotropic cuboid. The material orientation is fixed at $(\psi_1 = 45°, \beta_1 = 45°)$.

Please cite this article as: Chen C-S, et al. Three-dimensional stress intensity factors of a central square crack in a transversely isotropic cuboid with arbitrary material orientations. Eng Anal Bound Elem (2008), doi:10.1016/j.enganabound.2008.06.001

with their origin in the center of the cuboid. A square crack of $2a \times 2a$ is also located in the center of the cuboid, and a local coordinate system (x'', y'', z'') is attached to it with its z''-axis normal to the crack surface. The crack orientation is described by two angles: the inclined angle ψ_2 and dip orientation β_2, where ψ_2 is defined as the angle between the global horizontal $(x-y)$ plane and the crack plane (x'', y''), and β_2 as the angle between the global y-axis and the inclined angle plane.

The cracked finite cuboid is under a uniform normal tensile stress T applied at the top and bottom faces, as shown in Fig. 3. In the numerical example, the cuboid size is chosen to be $H/W = 2$ and the square size $2a/W = 0.5$. The material is a transversely isotropic marble and its elastic properties were obtained experimentally [32] as $E = 90$ GPa, $E' = 55$ GPa, $\nu = \nu' = 0.3$, $G = 35$ GPa, and $G' = 21$ GPa. After checking our program for a couple of special cases for accuracy, 40 and 36 nine-nodal quadrilateral elements were used to discretize the uncracked boundary and the crack surface, respectively, for the numerical examples presented below, with a relative error of 0.01 percent. Furthermore, the SIFs are plotted along the crack front using the four sides AB, BC, CD, and DA of the square, as shown in Fig. 3.

First, three types of materials, i.e., the transversely isotropic rocks with inclined angle and dip orientation $(\psi_1, \beta_1) = (0°, 0°)$, $(45°, 45°)$ and $(90°, 0°)$, and five types of crack inclined angle ψ_2 $(= 0°, 30°, 45°, 60°, 90°)$ $(\beta_2 = 0°)$ were selected to calculate the mode-I, mode-II, and mode-III SIFs along the sides of the crack. Shown in Fig. 4 is the variation of the normalized mode-I SIF (F_I) along the crack front for different crack angles when the material angles are fixed at $\psi_1 = 0°$, $\beta_1 = 0°$. As is expected, the SIFs are the same along all the four sides, reaching either a maximum or minimum in the middle of the side. It is also interesting that this maximum value changes substantially for varying crack angle, from 1.12 when the crack angle $\psi_2 = 0°$ to -0.432 when $\psi_2 = 90°$, passing the zero value when the crack angle is approximately at $\psi_2 = 60°$. The positive (negative) SIF value indicates that the crack is opened (closed) corresponding to the applied traction on the top (bottom) of the cuboid. Crack closure is actually a very common phenomenon and also an important issue in rock mechanics [33].

Shown in Fig. 5 is the variation of the normalized mode-II SIF (F_{II}) along the four sides of the crack front. Its variation is antisymmetric with respect to the corner C. In other words, the SIF along CDA can be obtained from that along ABC by simply changing the sign. It is also observed that the maximum value of F_{II} is equal to 0.419 in AB when the crack angle $\psi_2 = 45°$, and it is zero when $\psi_2 = 0°$ and 90°. This indicates that when $\psi_2 = 0°$ and 90°, the crack is under pure tensile and compressive loading, respectively. It is also interesting that for any crack angle, the magnitude of F_{II} along BC or DA is much smaller, at 0.079, as compared to its maximum value along AD and CD at 0.419. Due to the symmetric property, the mode-III SIF follows a similar trend as mode-II SIF, only the two horizontal axes being switched $(x'' \leftrightarrow y'')$, Fig. 3).

Fig. 6 shows the variation of the normalized mode-I SIF F_I in the transversely isotropic material with inclined angle $\psi_1 = 45°$ and dip orientation $\beta_1 = 45°$, along the square crack front, for different crack angles $\psi_2 = 0°$, 30°, 45°, 60°, and 90° $(\beta_2 = 0°)$. It is

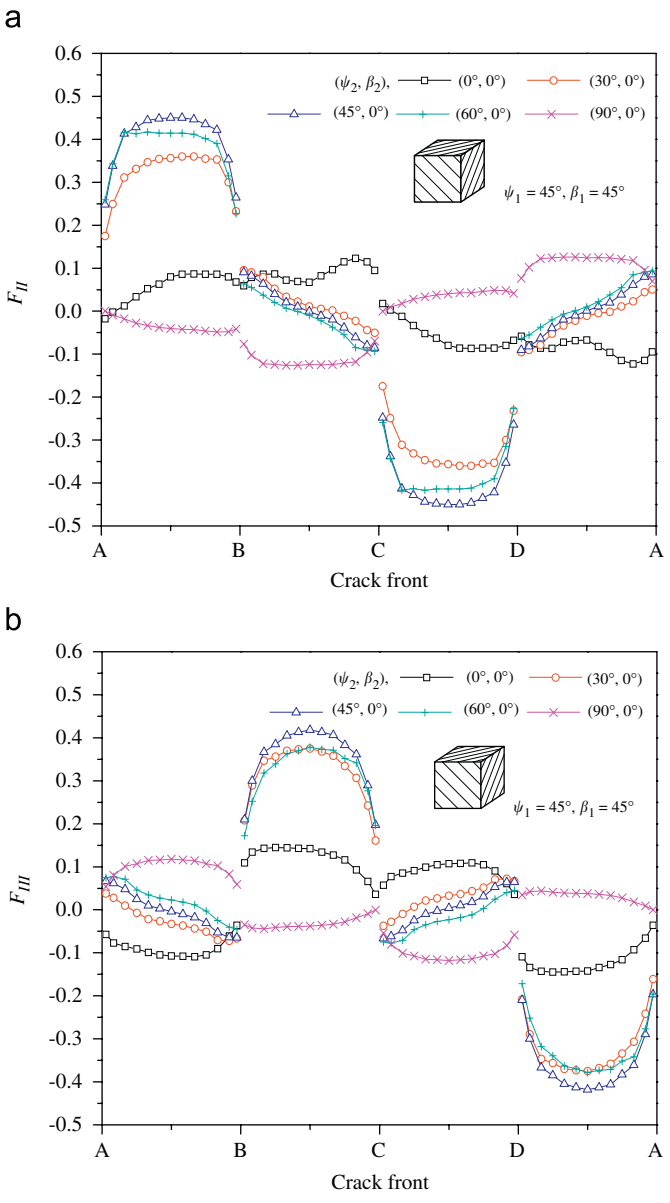

Fig. 7. (a) The normalized mode-II SIF along the square-shaped crack fronts AB, BC, CD, and DA for different crack orientation (ψ_2, β_2) within a finite transversely isotropic cuboid. The material orientation is fixed at $(\psi_1 = 45°, \beta_1 = 45°)$. (b) The normalized mode-III SIF along the square-shaped crack fronts AB, BC, CD, and DA for different crack orientation (ψ_2, β_2) within a finite transversely isotropic cuboid. The material orientation is fixed at $(\psi_1 = 45°, \beta_1 = 45°)$.

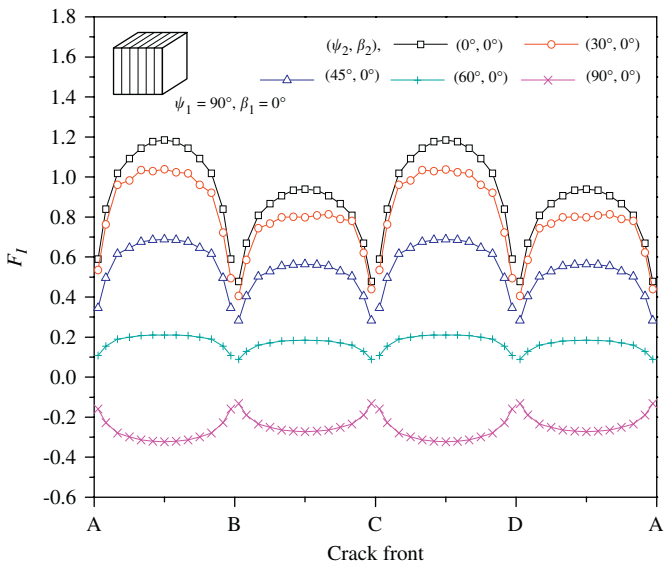

Fig. 8. The normalized mode-I SIF along the square-shaped crack fronts AB, BC, CD, and DA for different crack orientation (ψ_2, β_2) within a finite transversely isotropic cuboid. The material orientation is fixed at $(\psi_1 = 90°, \beta_1 = 0°)$.

Please cite this article as: Chen C-S, et al. Three-dimensional stress intensity factors of a central square crack in a transversely isotropic cuboid with arbitrary material orientations. Eng Anal Bound Elem (2008), doi:10.1016/j.enganabound.2008.06.001

observed that the SIF F_I is the same along the crack fronts ABC and CDA, and that its maximum value for this material type is larger than that for the material case with $\psi_1 = 0^\circ$ and $\beta_1 = 0^\circ$ (1.4 in Fig. 6 vs. 1.12 in Fig. 4). Furthermore, similar to Fig. 4, the maximum SIF value along each side decreases with increasing dip angle ψ_2. It reaches zero when the dip angle is somewhere between 60° and 90°; then, it comes negative, corresponding to the crack closure. Figs. 7a and b show, respectively, the variation of the normalized SIFs F_{II} and F_{III} in the material with angles $\psi_1 = 45^\circ$ and $\beta_1 = 45^\circ$, along the square crack front, for different crack angles $\psi_2 = 0^\circ$, 30°, 45°, 60°, and 90° ($\beta_2 = 0^\circ$). It is observed that the SIF values for the shear and tearing modes along the crack front ABC are antisymmetric as compared to those along CDA. It is further noticed that the maximum SIF for F_{II} is reached along the crack fronts AB and CD, whilst for F_{III}, the maximum is along BC and DA.

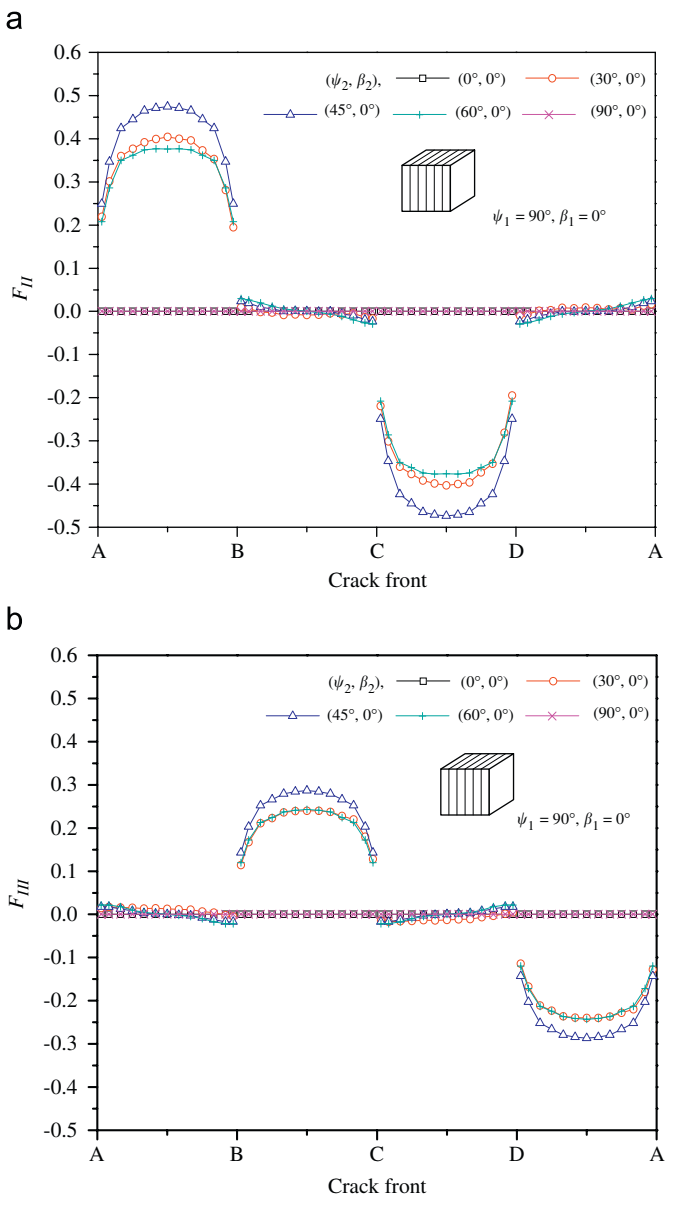

Fig. 9. (a) The normalized mode-II SIF along the square-shaped crack fronts AB, BC, CD, and DA for different crack orientation (ψ_2, β_2) within a finite transversely isotropic cuboid. The material orientation is fixed at $(\psi_1 = 90^\circ, \beta_1 = 0^\circ)$. (b)The normalized mode-III SIF along the square-shaped crack fronts AB, BC, CD, and DA for different crack orientation (ψ_2, β_2) within a finite transversely isotropic cuboid. The material orientation is fixed at $(\psi_1 = 90^\circ, \beta_1 = 0^\circ)$.

The variation of the SIFs along the crack front for the other material case is shown in Figs. 8 and 9, where the material orientation angles are $\psi_1 = 90^\circ$ and $\beta_1 = 0^\circ$, and the crack angles are $\psi_2 = 0^\circ$, 30°, 45°, 60°, and 90° ($\beta_2 = 0^\circ$). Comparing Fig. 8 to Fig. 4, we noted that while in Fig. 4, the SIFs of mode-I are the same along each side of the square, in Fig. 8, they are the same along sides AB and CD, and the same along BC and DA. Furthermore, the maximum SIF along AB and CD is larger than that along BC and DA (1.185 vs. 0.94), with these two values being, respectively, larger and smaller than those in Fig. 4. This different phenomenon is due to the fact that in Fig. 8 the material isotropic plane is normal to the crack plane, whilst in Fig. 4 both planes are parallel to each other.

Figs. 9a and b show, respectively, the corresponding variation of the normalized SIFs F_{II} and F_{III} with material angles $\psi_1 = 90^\circ$ and $\beta_1 = 0^\circ$, along the square crack front, for different crack angles $\psi_2 = 0^\circ$, 30°, 45°, 60°, and 90° ($\beta_2 = 0^\circ$). Again, we observed that the SIF values for the shear and tearing modes along the crack front ABC are antisymmetric as compared to those along CDA. It is further noticed that the maximum SIF for F_{II} is reached along the crack fronts AB and CD, whilst for F_{III}, the maximum is along BC and DA. Furthermore, the magnitude of the maximum in F_{II} is larger than that in F_{III} (0.474 vs. 0.287), due to the different orientation relations between the crack fronts and the material isotropic plane.

We have also run our program for another case where the material orientation angles are $\psi_1 = \beta_1 = 45^\circ$, but the crack angles are $(\psi_2, \beta_2) = (30^\circ, 0^\circ), (30^\circ, 30^\circ), (30^\circ, 60^\circ), (60^\circ, 0^\circ), (60^\circ, 30^\circ)$, and $(60^\circ, 60^\circ)$ (Figs. 10 and 11a, b). It is observed from Fig. 10 that the crack inclined angle ψ_2 is an important factor in the mode-I SIF. It is obvious that the SIF values are much larger for $\psi_2 = 30^\circ$ than those for $\psi_2 = 60^\circ$, independent of the crack dip orientation β_2. Furthermore, for fixed $\psi_2 = 30^\circ$, the SIF value increases with increasing dip orientation β_2. Figs. 11a and b show the corresponding F_{II} and F_{III} along the crack front. As can be seen, the variation of F_{II} and F_{III} is much more complicated than that of F_I, although they still possess the antisymmetric feature. In other words, the SIF values along the crack front ABC have the same magnitude but opposite sign as compared to those along CDA.

Finally, shown in Figs. 12a–c are the relative CODs. Fig. 12a is for the material angles $\psi_1 = \beta_1 = 0^\circ$ and crack angles $\psi_2 = \beta_2 = 0^\circ$. It is apparent that for this case, the crack is under a uniform pure tensile

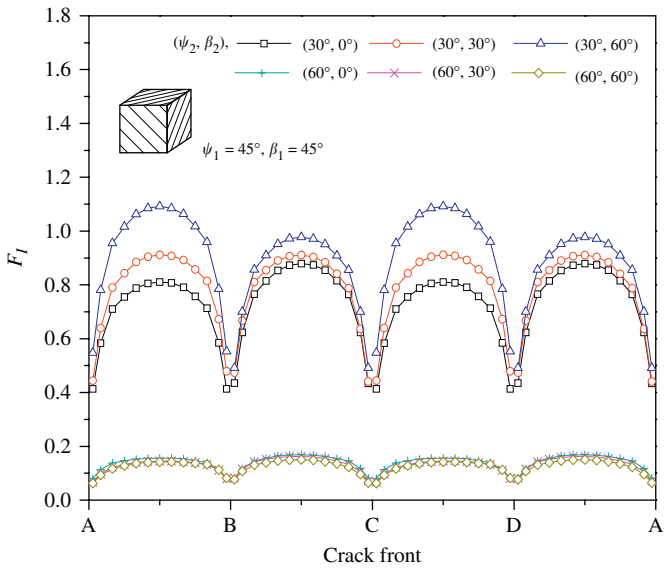

Fig. 10. The normalized mode-I SIF along the square-shaped crack fronts AB, BC, CD, and DA for different crack orientation (ψ_2, β_2) within a finite transversely isotropic cuboid. The material orientation is fixed at $(\psi_1 = 45^\circ, \beta_1 = 45^\circ)$.

Please cite this article as: Chen C-S, et al. Three-dimensional stress intensity factors of a central square crack in a transversely isotropic cuboid with arbitrary material orientations. Eng Anal Bound Elem (2008), doi:10.1016/j.enganabound.2008.06.001

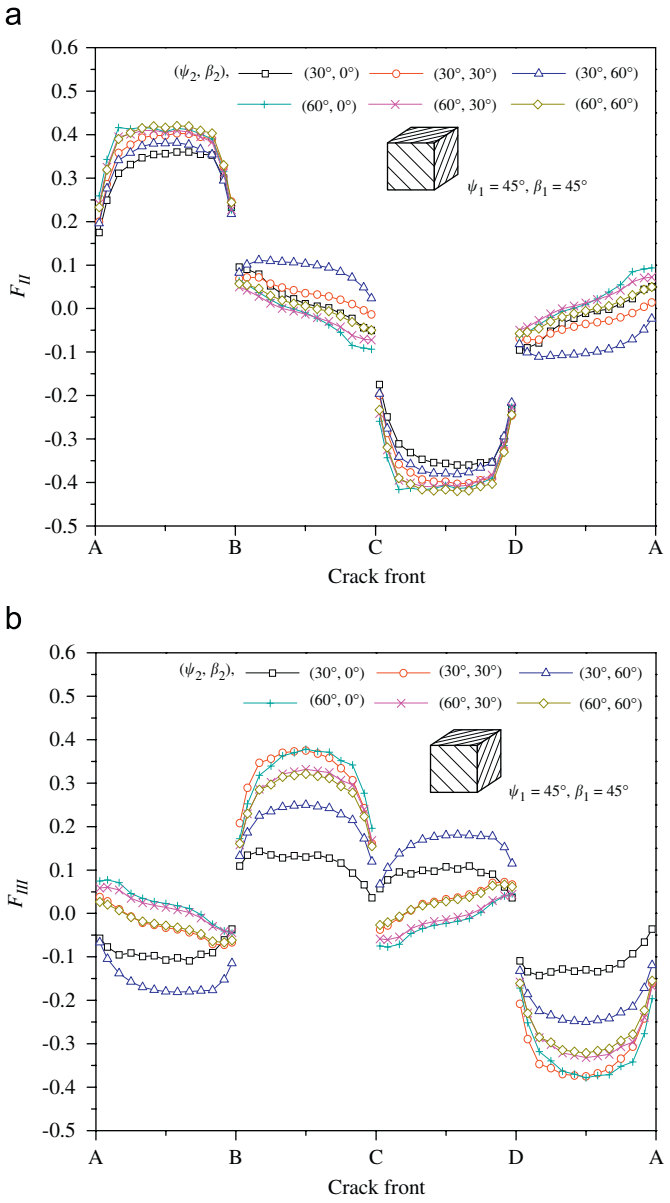

Fig. 11. (a) The normalized mode-II SIF along the square-shaped crack fronts AB, BC, CD, and DA for different crack orientation (ψ_2, β_2) within a finite transversely isotropic cuboid. The material orientation is fixed at $(\psi_1 = 45°, \beta_1 = 45°)$. (b) The normalized mode-III SIF along the square-shaped crack fronts AB, BC, CD, and DA for different crack orientation (ψ_2, β_2) within a finite transversely isotropic cuboid. The material orientation is fixed at $(\psi_1 = 45°, \beta_1 = 45°)$.

stress in the vertical direction and one observes only the opening COD (there is no shearing displacement). However, in Fig. 12b, where the material angles $\psi_1 = \beta_1 = 0°$ but the crack angles $\psi_2 = 90°$ and $\beta_2 = 0°$, the relative COD is negative (shown in Fig. 12b is the magnitude of the relative COD), implying that the crack surface is under a pure compression. When the material angles $\psi_1 = 45°$, $\beta_1 = 45°$ and crack angles $\psi_2 = 45°$ and $\beta_2 = 45°$, one observes not only a relative COD in the normal direction of the crack, but also a relative shear displacement, as shown in Fig. 12c for the relative shearing displacement.

6. Conclusions

We applied the dual-BEM or the single-domain BEM to the analysis of mixed 3D SIFs in a finite and transversely isotropic solid containing an internal square crack. A set of four special nine-node quadrilateral elements are employed to approximate the crack surface as well as the outer boundary. The mixed 3D SIFs are evaluated using the asymptotic relation between the SIFs and the relative CODs via the Barnett–Lothe tensor. Numerical examples of the mixed 3D SIFs are presented for a transversely isotropic and cracked rock cuboid with any given material orientation. The cuboid is under a uniform vertical traction along its top and bottom surfaces and the central square crack is arbitrarily oriented. Our results show that among the selected material and crack orientations, the mode-I SIF reaches the largest possible value when the material inclined angle $\psi_1 = 45°$ and dig angle $\beta_1 = 45°$, and the crack inclined angle $\psi_2 = 0°$ and dig angle $\beta_2 = 0°$. It is further observed that when the crack is oriented vertically or nearly vertically, the mode-I SIF becomes negative, indicating that the crack closes due to an overall compressive loading normal to the crack surface. Variation of the SIFs for modes II and III along the crack fronts also shows some interesting features for different combinations of the material and crack orientations, which could be useful in the future failure analysis and design of cracked anisotropic solids.

Acknowledgement

The work of E.P. was partially supported by ARL and AFRL. We thank Prof. Xu Wang for his constructive discussion and the reviewers and editor for their beneficial comments and suggestions.

Appendix A

The anisotropic elastic compliance $[a]$ as functions of the elastic constants (E, E', ν, ν', and G') and the inclined angle (ψ_1) with fixed $\beta_1 = 0°$

$$a_{11} = \sin^2\psi_1\left(\frac{\sin^2\psi_1}{E'} - \frac{\nu'}{E}\cos^2\psi_1\right) + \cos^2\psi_1 \times \left(-\frac{\nu'}{E}\sin^2\psi_1 + \frac{\cos^2\psi_1}{E}\right) + \frac{\sin^2 2\psi_1}{4G'}$$

$$a_{12} = -\frac{\nu'}{E}\sin^2\psi_1 - \frac{\nu}{E}\cos^2\psi_1$$

$$a_{13} = \sin^2\psi_1\left(\frac{\cos^2\psi_1}{E'} - \frac{\nu'}{E}\sin^2\psi_1\right) + \cos^2\psi_1 \times \left(-\frac{\nu'}{E}\cos^2\psi_1 + \frac{\sin^2\psi_1}{E}\right) - \frac{\sin^2 2\psi_1}{4G'}$$

$$a_{15} = -\sin 2\psi_1 \sin^2\psi_1\left(\frac{1}{E'} + \frac{\nu'}{E}\right) + \sin 2\psi_1 \cos^2\psi_1 \times \left(\frac{1}{E} + \frac{\nu'}{E}\right) - \frac{\sin 2\psi_1 \cos 2\psi_1}{2G'}$$

$$a_{22} = \frac{1}{E}$$

$$a_{23} = -\frac{\nu'}{E}\cos^2\psi_1 - \frac{\nu}{E}\sin^2\psi_1$$

$$a_{25} = \sin 2\psi_1\left(\frac{\nu'}{E'} - \frac{\nu}{E}\right)$$

$$a_{33} = \cos^2\psi_1\left(\frac{\cos^2\psi_1}{E'} - \frac{\nu'}{E}\sin^2\psi_1\right) + \sin^2\psi_1 \times \left(-\frac{\nu'}{E}\cos^2\psi_1 + \frac{\sin^2\psi_1}{E}\right) + \frac{\sin^2 2\psi_1}{4G'}$$

$$a_{35} = -\sin 2\psi_1 \cos^2\psi_1\left(\frac{1}{E'} + \frac{\nu'}{E}\right) + \sin 2\psi_1 \sin^2\psi_1 \times \left(\frac{1}{E} + \frac{\nu'}{E}\right) + \frac{\sin 2\psi_1 \cos 2\psi_1}{2G'}$$

Please cite this article as: Chen C-S, et al. Three-dimensional stress intensity factors of a central square crack in a transversely isotropic cuboid with arbitrary material orientations. Eng Anal Bound Elem (2008), doi:10.1016/j.enganabound.2008.06.001

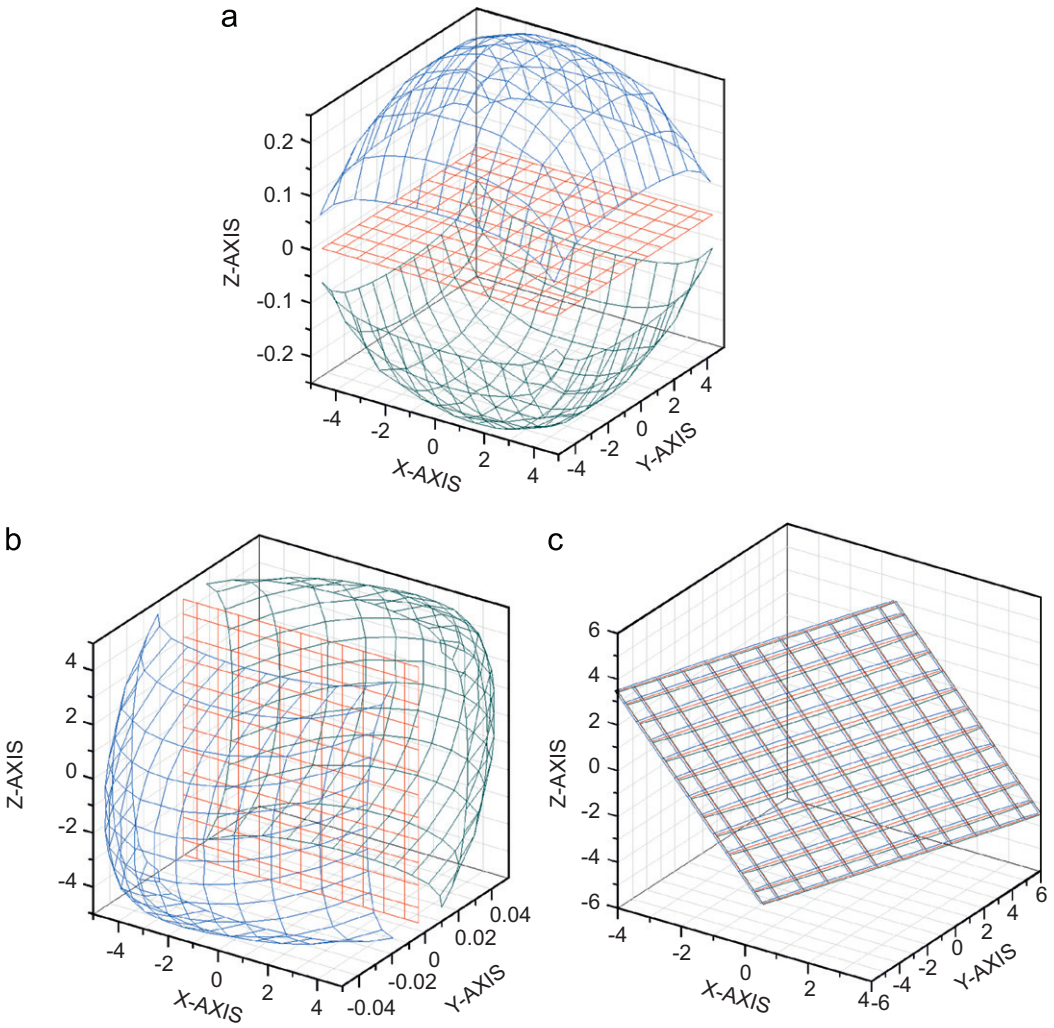

Fig. 12. (a) Opening of the square crack under a uniform vertical tensile stress applied at the top and bottom surface of the cuboid. The material orientation is $(\psi_1 = 0^\circ, \beta_1 = 0^\circ)$ and the crack orientation is $(\psi_2 = 0^\circ, \beta_2 = 0^\circ)$. (b) Closure of the square crack under a uniform vertical tensile stress applied at the top and bottom surface of the cuboid. The material orientation is $(\psi_1 = 0^\circ, \beta_1 = 0^\circ)$ and the crack orientation is $(\psi_2 = 90^\circ, \beta_2 = 0^\circ)$. (c) Shearing of the square crack under a uniform vertical tensile stress applied at the top and bottom surface of the cuboid. The material orientation is $(\psi_1 = 0^\circ, \beta_1 = 0^\circ)$ and the crack orientation is $(\psi_2 = 45^\circ, \beta_2 = 45^\circ)$.

$$a_{44} = \frac{\sin^2\psi_1}{G} + \frac{\cos^2\psi_1}{G'}$$
$$a_{46} = \sin\psi_1 \cos\psi_1 \left(\frac{1}{G} - \frac{1}{G'}\right)$$
$$a_{55} = \sin^2 2\psi_1 \left(\frac{1}{E'} + \frac{1}{E} + 2\frac{\nu'}{E}\right) + \frac{\cos^2 2\psi_1}{G'}$$
$$a_{66} = \frac{\cos^2\psi_1}{G} + \frac{\sin^2\psi_1}{G'}$$
$$a_{14} = a_{16} = a_{24} = a_{26} = a_{34} = a_{36} = a_{45} = a_{56} = 0 \quad \text{(A.1)}$$

Appendix B

Shape functions for the four special elements
Shape functions for type-I element

$$\phi_1 = 0.25\xi_1\xi_2(\xi_1 - 1)(\xi_2 - 1)$$
$$\phi_2 = 0.5\xi_2(1 - \xi_1^2)(\xi_2 - 1)$$
$$\phi_3 = 0.25\xi_1\xi_2(\xi_1 + 1)(\xi_2 - 1)$$
$$\phi_4 = 0.5\xi_1(\xi_1 - 1)(1 - \xi_2^2)$$
$$\phi_5 = (1 - \xi_1^2)(1 - \xi_2^2)$$
$$\phi_6 = 0.5\xi_1(\xi_1 + 1)(1 - \xi_2^2)$$
$$\phi_7 = 0.25\xi_1\xi_2(\xi_1 - 1)(\xi_2 + 1)$$
$$\phi_8 = 0.5\xi_2(1 - \xi_1^2)(\xi_2 + 1)$$
$$\phi_9 = 0.25\xi_1\xi_2(\xi_1 + 1)(\xi_2 + 1) \quad \text{(B.1)}$$

Shape functions for type-II element

$$\phi_1 = 0.45\xi_1\xi_2(\xi_1 - 1)(\xi_2 - 1)$$
$$\phi_2 = 0.9\xi_2(1 - \xi_1^2)(\xi_2 - 1)$$
$$\phi_3 = 0.45\xi_1\xi_2(\xi_1 + 1)(\xi_2 - 1)$$
$$\phi_4 = 0.75\xi_1(\xi_1 - 1)(1 - \xi_2)\left(\tfrac{2}{3} + \xi_2\right)$$
$$\phi_5 = 1.5(\xi_1^2 - 1)(\xi_2 - 1)\left(\tfrac{2}{3} + \xi_2\right)$$
$$\phi_6 = 0.75\xi_1(\xi_1 + 1)(1 - \xi_2)\left(\tfrac{2}{3} + \xi_2\right)$$
$$\phi_7 = 0.3\xi_1\xi_2(\xi_1 - 1)\left(\tfrac{2}{3} + \xi_2\right)$$
$$\phi_8 = 0.6\xi_2(1 - \xi_1^2)\left(\tfrac{2}{3} + \xi_2\right)$$
$$\phi_9 = 0.3\xi_1\xi_2(\xi_1 + 1)\left(\tfrac{2}{3} + \xi_2\right) \quad \text{(B.2)}$$

Shape functions for type-III element

$$\phi_1 = 0.81\xi_1\xi_2(\xi_1 - 1)(\xi_2 - 1)$$
$$\phi_2 = 1.35\xi_2(1 - \xi_1)\left(\tfrac{2}{3} + \xi_1\right)(\xi_2 - 1)$$
$$\phi_3 = 0.54\xi_1\xi_2\left(\tfrac{2}{3} + \xi_1\right)(\xi_2 - 1)$$

Please cite this article as: Chen C-S, et al. Three-dimensional stress intensity factors of a central square crack in a transversely isotropic cuboid with arbitrary material orientations. Eng Anal Bound Elem (2008), doi:10.1016/j.enganabound.2008.06.001

$$\phi_4 = 1.35\xi_1(\xi_1 - 1)(1 - \xi_2)\left(\tfrac{2}{3} + \xi_2\right)$$
$$\phi_5 = 2.25(1 - \xi_1)\left(\tfrac{2}{3} + \xi_1\right)(1 - \xi_2)\left(\tfrac{2}{3} + \xi_2\right)$$
$$\phi_6 = 0.9\xi_1\left(\tfrac{2}{3} + \xi_1\right)(1 - \xi_2)\left(\tfrac{2}{3} + \xi_2\right)$$
$$\phi_7 = 0.54\xi_1\xi_2(\xi_1 - 1)\left(\tfrac{2}{3} + \xi_2\right)$$
$$\phi_8 = 0.9\xi_2(1 - \xi_1)\left(\tfrac{2}{3} + \xi_1\right)\left(\tfrac{2}{3} + \xi_2\right)$$
$$\phi_9 = 0.36\xi_1\xi_2\left(\tfrac{2}{3} + \xi_1\right)\left(\tfrac{2}{3} + \xi_2\right) \quad \text{(B.3)}$$

Shape functions for type-IV element

$$\phi_1 = 0.54\xi_1\xi_2\left(\xi_1 - \tfrac{2}{3}\right)(\xi_2 - 1)$$
$$\phi_2 = -1.35\xi_2(1 - \xi_1)\left(\xi_1 - \tfrac{2}{3}\right)(\xi_2 - 1)$$
$$\phi_3 = 0.81\xi_1\xi_2(\xi_1 + 1)(\xi_2 - 1)$$
$$\phi_4 = 0.9\xi_1\left(\xi_1 - \tfrac{2}{3}\right)(1 - \xi_2)\left(\tfrac{2}{3} + \xi_2\right)$$
$$\phi_5 = -2.25(1 + \xi_1)\left(\xi_1 - \tfrac{2}{3}\right)(1 - \xi_2)\left(\tfrac{2}{3} + \xi_2\right)$$
$$\phi_6 = 1.35\xi_1(\xi_1 + 1)(1 - \xi_2)\left(\tfrac{2}{3} + \xi_2\right)$$
$$\phi_7 = 0.36\xi_1\xi_2\left(\xi_1 - \tfrac{2}{3}\right)\left(\tfrac{2}{3} + \xi_2\right)$$
$$\phi_8 = -0.9\xi_2(1 + \xi_1)\left(\xi_1 - \tfrac{2}{3}\right)\left(\tfrac{2}{3} + \xi_2\right)$$
$$\phi_9 = 0.54\xi_1\xi_2(\xi_1 + 1)\left(\tfrac{2}{3} + \xi_2\right) \quad \text{(B.4)}$$

References

[1] Griffith AA. The phenomena of rupture and flow in solids. Phil Trans R Soc A 1920;221:163–98.
[2] Irwin GR. Analysis of stresses and strains near the end of a crack traversing a plate. J Appl Mech 1957;24:361–4.
[3] Singh R, Carter BJ, Wawrzynek PA, Ingraffea AR. Universal crack closure integral for SIF estimation. Eng Fract Mech 1998;60(2):133–46.
[4] Pan E, Yuan FG. Boundary element analysis of three-dimensional cracks in anisotropic solids. Int J Num Methods Eng 2000;48:211–37.
[5] Lazarus V, Leblond JB, Mouchrif SE. Crack front rotation and segmentation in mixed mode I+III or I+II+III. Part I: calculation of stress intensity factors. J Mech Phys Solids 2001;49:1399–420.
[6] Zhou W, Lim KM, Lee KH, Tay AAO. A new variable-order singular boundary element for calculating stress intensity factors in three-dimensional elasticity problems. Int J Solids Struct 2005;42:159–85.
[7] Yue ZQ, Xiao HT, Pan E. Stress intensity factors of square crack inclined to interface of transversely isotropic bi-material. Eng Anal Boundary Element 2007;31:50–65.
[8] Hong HK, Chen JT. Derivations of integral equations of elasticity. J Eng Mech ASCE 1988;114(6):1028–44.
[9] Chen JT, Hong HK. Review of dual boundary element methods with emphasis on hypersingular integrals and divergent series. Appl Mech Rev ASME 1999; 52(1):17–33.
[10] Ariza MP, Dominguez J. Dynamic BE, analysis of 3-D cracks in transversely isotropic solids. Comput Meth Appl Mech Eng 2004;193:765–79.
[11] Liu Y, Liang LH, Hong QC, Antes H. Non-linear surface crack analysis by three dimensional boundary element with mixed boundary conditions. Eng Fract Mech 1999;63:413–24.
[12] Hatzigeorgiou GD, Beskos DE. Static analysis of 3D damaged solids and structures by BEM. Eng Anal Boundary Element 2002;26:521–6.
[13] Partheymüller P, Haas M, Kuhn G. Comparison of the basic and the discontinuity formulation of the 3D-dual boundary element method. Eng Anal Boundary Element 2000;24:777–88.
[14] Popov V, Power H, Walker SP. Numerical comparison between two possible multipole alternatives for the BEM solution of 3D elasticity problems based upon Taylor series expansions. Eng Anal Boundary Element 2003;27:521–31.
[15] Zhao MH, Fan CY, Liu T, Yang F. Extended displacement discontinuity Green's functions for three-dimensional transversely isotropic magneto-electro-elastic media and applications. Eng Anal Boundary Element 2007;31:547–58.
[16] Lo SH, Dong CY, Cheung YK. Integral equation approach for 3D multiple-crack problems. Eng Fract Mech 2005;72:1830–40.
[17] dell'Erba DN, Aliabadi MH. On the solution of three-dimensional thermo-elastic mixed-mode edge crack problems by the dual boundary element method. Eng Fract Mech 2000;66:269–85.
[18] Blackburn WS. Three dimensional calculation of growth of cracks starting in parallel planes by boundary elements. Int J Fatigue 1999;21:933–9.
[19] Rundamornrat J. Analysis of 3D cracks in anisotropic multi-material domain with weakly singular SGBEM. Eng Anal Boundary Element 2006;30:834–46.
[20] Rungamornrat J, Mear ME. Weakly-singular, weak-form integral equations for cracks in three-dimensional anisotropic media. Int J Solids Struct 2008;45: 1283–301.
[21] Noda NA, Xu C. Controlling parameter of the stress intensity factors for a planar interfacial crack in three-dimensional bimaterials. Int J Solids Struct 2008;45(3/4):1017–31.
[22] Dorogoy A, Banks-Sills L. Effect of crack face contact and friction on Brazilian disk specimens—a finite difference solution. Eng Fract Mech 2005;72(18): 2758–73.
[23] Altus E. The finite difference technique for solving crack problems. Eng Fract Mech 1984;19(5):947–57.
[24] Chen YM. Numerical computation of dynamic stress intensity factors by a Lagrangian finite-difference method (the HEMP code). Eng Fract Mech 1975;7(4):653–60.
[25] Leung AYT, Su RKL. A numerical study of singular stress field of 3D cracks. Finite Element Anal Des 1995;18:389–401.
[26] He WJ, Lin Y, Ding HJ. A three-dimensional formula for determining stress intensity factors in finite element analysis of cracked bodies. Eng Fract Mech 1997;57(4):409–15.
[27] Goodman RE. Introduction to Rock Mechanics. New York: Wiley; 1980.
[28] Pan E. A general boundary element analysis of 2-D linear elastic fracture mechanics. Int J Fract 1997;88:41–59.
[29] Pan E, Amadei B. Fracture mechanics analysis of cracked 2-D anisotropic media with a new formulation of the boundary element method. Int J Fract 1996;77:161–74.
[30] Pan E, Amadei B. A 3-D boundary element formulation of anisotropic elasticity with gravity. Appl Math Modelling 1996;20:114–20.
[31] Ting TCT. Anisotropic elasticity: theory and applications. Oxford: Oxford University Press; 1996.
[32] Chen CS, Pan E, Amadei B. Determination of deformability and tensile strength of anisotropic rock using Brazilian tests. Int J Rock Mech Min Sci 1998;35(1):43–61.
[33] Chang SH, Lee CI, Lee YK. An experimental damage model and its application to the evaluation of the excavation damage zone. Rock Mech Rock Eng 2007;40(3):245–85.

Please cite this article as: Chen C-S, et al. Three-dimensional stress intensity factors of a central square crack in a transversely isotropic cuboid with arbitrary material orientations. Eng Anal Bound Elem (2008), doi:10.1016/j.enganabound.2008.06.001